

Supplemental material to Dunkel et al.: Highly stressed lower crust: Evidence from dry pseudotachylytes in granulites, Lofoten Archipelago, Northern Norway

1. Localities, from south to north:

REI: Roadcut south of the tunnel Ramsviktunnelen (close to the village of Reine) (latitude: 67.91826, longitude: 13.08114). Monzodioritic.

HAM: Two roadcuts, one on the small island of Hamnøya (67.94559, 13.13568), the other one at a distance of ca 500 m just north of Hamnøya (67.94916, 13.13722). These are discussed together in the manuscript. Monzonitic and gabbroic.

ØL: Roadcut along the road north of Reine, between two short roofed sections of the road, south of Ølkonvatnet (67.96589, 13.16921). Gabbroic.

HIL: Small quarry just west of the bridge over Kåkersundet (68.01773, 13.17551). Gabbroic, biotite-bearing.

2. Methods:

Electron backscatter images were acquired on a Hitachi SU5000 FE-SEM (Department of Geosciences, University of Oslo, Norway). Major element compositions were measured by wavelength-dispersive spectrometry (WDS) with a Cameca SX 100 electron microprobe (Department of Geosciences, University of Oslo, Norway), using an acceleration voltage of 15 kV and beam currents between 10 and 20 nA.

Whole-rock geochemical analysis was conducted at Activation Labs in Ontario (their 4Lithores package). The fused samples were diluted and analyzed by Perkin Elmer Sciex ELAN 6000, 6100 or 9000 ICP-MS. Calibration was performed using 10 synthetic calibration standards. A set of 10 certified reference material was run before and after every batch of

samples. Duplicates were fused and analyzed every 17 samples. Instrument was recalibrated every 2 trays of samples.

Elastic geobarometry on quartz inclusions in garnet were performed following the procedure outlined by Zhong et al. (2019). Raman spectra were acquired with a Horiba Jobin-Yvon (T64000) Raman spectrometer located at the Department of Chemistry, University of Oslo, using a single crystal quartz standard for calibration. The standard deviation (1σ) of the standard shift was less than 0.2 cm^{-1} . The Raman spectra were fitted with a Gaussian-Lorentzian equation using the MATLAB function “*lsqcurvefit*”. The 464 and 128 cm^{-1} Raman band positions were used for the elastic geobarometry. The PVT relationship for quartz is from Angel et al. (2017) and that for garnet from Milani et al. (2015). The equation to calculate residual pressure is based on the following relationship (Guiraud and Powell 2006).

$$P_{\text{inc}} = \frac{4G}{3} \left(\frac{V_{\text{inc}}^{25^{\circ}\text{C}, P_{\text{inc}}}}{V_{\text{inc}}^{T_{\text{etp}}, P_{\text{etp}}}} - \frac{V_{\text{host}}^{25^{\circ}\text{C}, 1\text{bar}}}{V_{\text{host}}^{T_{\text{etp}}, P_{\text{etp}}}} \right),$$

where P_{inc} is the residual pressure of the quartz inclusion, G is the shear modulus of the garnet host, $V_{\text{inc}}^{25^{\circ}\text{C}, P_{\text{inc}}}$ is the specific volume of the inclusion at room temperature and residual pressure, $V_{\text{inc}}^{T_{\text{etp}}, P_{\text{etp}}}$ is the inclusion volume at entrapment P - T , and $V_{\text{host}}^{25^{\circ}\text{C}, 1\text{bar}}$ is the garnet host specific volume at room P - T .

3. Figures:

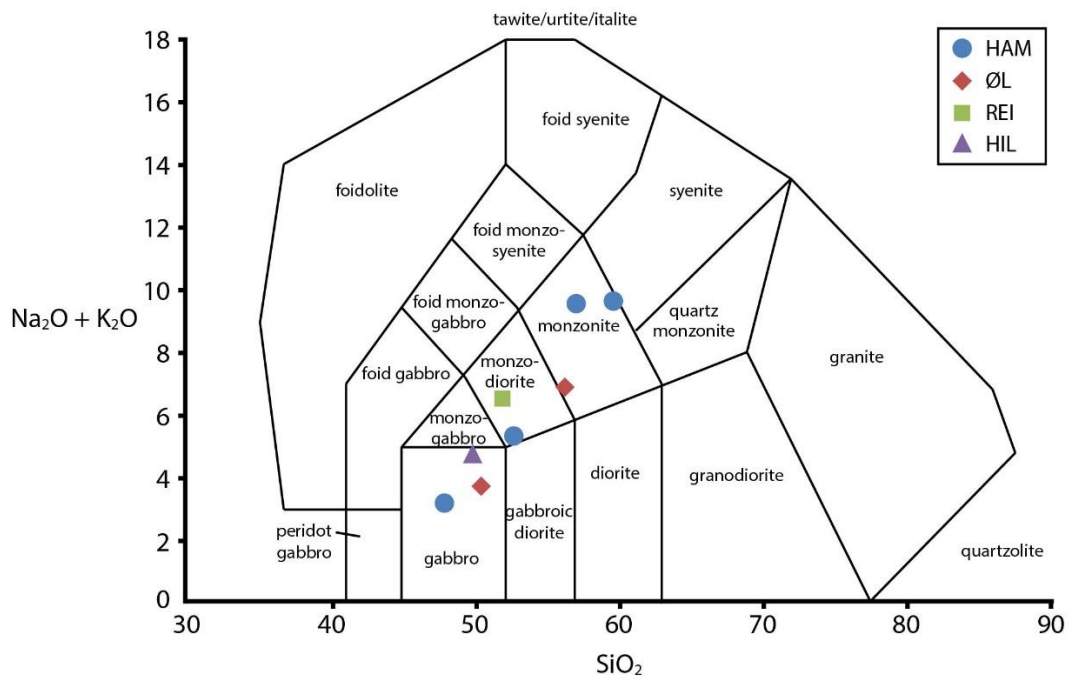


Fig. S1: TAS-diagram showing the range of compositions between gabbro and monzonite.

Compositional fields redrawn from Middlemost (1994).

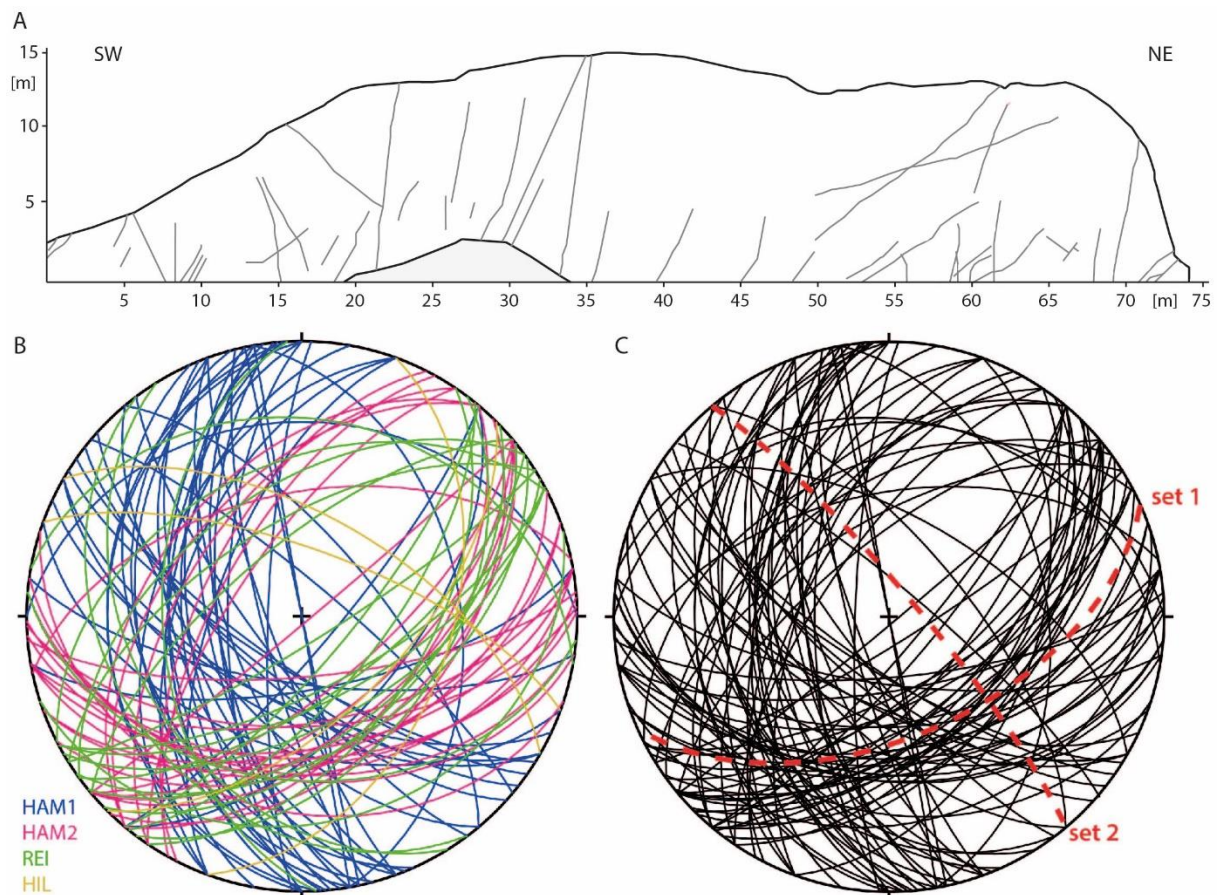


Fig. S2: A: Sketch of outcrop HAM1 (north of Hamnøya) with pseudotachylytes. The host rock is monzonite. B and C: Orientations of pseudotachylytes from Moskenesøya in lower hemisphere projections. B: Orientations of pseudotachylytes measured in four outcrops on Moskenesøya. The reason that certain orientations have only been measured in one outcrop is the orientations of those subvertical roadcuts. Outcrop HAM1, for example, is subparallel to the most common pseudotachylyte orientation in HAM2, so that those orientations were not observed in HAM1. C: Similarity between the orientations from Mosksnesøya and the two main structural orientations from Nusfjord East (Campbell et al., 2020) shown in red.

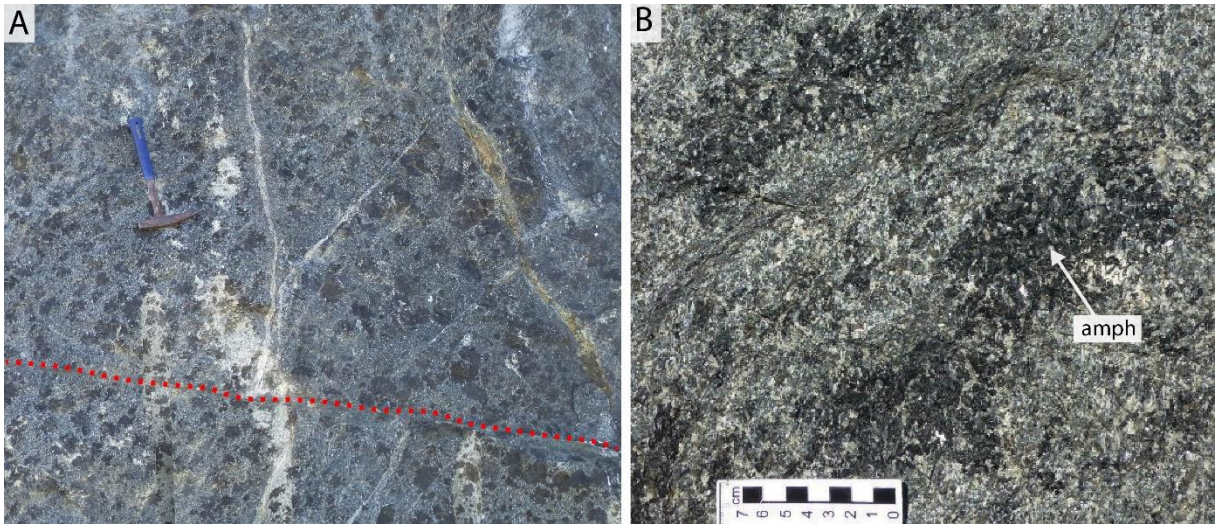


Fig. S3: Amphibolitization of gabbros at ØL. A) Patchy distribution of dark amphibole, unrelated to the thin pseudotachylyte fault vein (red line). The wide white area is a surface feature. B) Close-up on some of the amphibole (amph) patches.

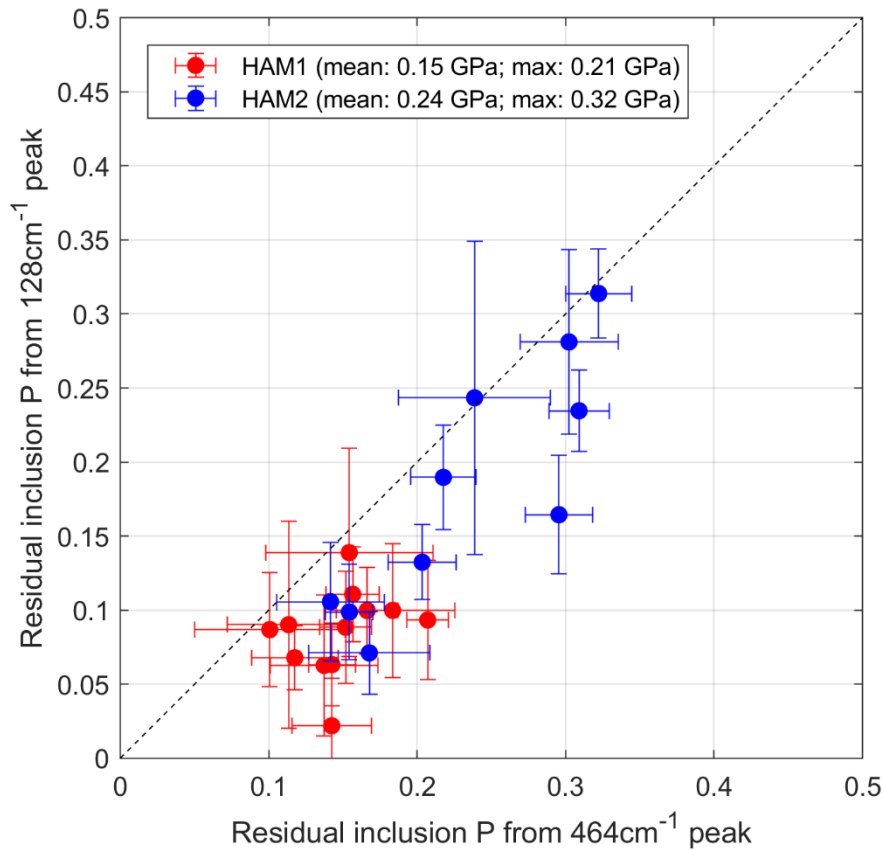


Fig. S4: Residual pressures of quartz inclusions in garnet from samples HAM-1 and HAM-2, calculated from the 464 and 128 cm^{-1} Raman band positions. The residual inclusion pressure yielded by the 464 cm^{-1} band is consistently higher than that of the 128 cm^{-1} band by ca. 0.05 GPa. This phenomenon has been observed in several studies including Gonzalez et al. (2019) and Zhong et al. (2019). This has been interpreted to be due to the elastic anisotropy of the quartz inclusion (Murri et al. 2018). In the calibrating experiments relating Raman shift and pressure (Schmidt and Ziemann 2000), only hydrostatic stress is externally applied to a quartz crystal, whereas natural quartz inclusions preserved in garnet are under non-hydrostatic stress. This leads to a discrepancy between the pressures determined from different bands. However, its effect on the recovered entrapment pressure has been shown to be insignificant (<0.1 GPa) for amphibolite and eclogite facies conditions (Murri et al. 2018). The errors are relatively large because the cauliflower garnet hosts are very “cloudy”, which leads to weak Raman signal of the quartz inclusions.

4. Tables:

Tab. S1: Whole rock geochemistry of samples from Moskenesøya. Note especially the similarities in composition between host rock and pseudotachylyte (pst) for samples HAM-3 and ØL-5. (The amphibole-rich patches at ØL, as shown in Suppl. Fig. 4, were not sampled.)

Sample	HAM-3 host rock	HAM-3 pst	HAM-4 host rock	HAM-9 host rock	HAM-12 host rock	ØL-3 host rock	ØL-5 host rock	ØL-5 pst	REI-1 host rock	HIL-3 host rock
Major elements (wt%)										
SiO ₂	59.68	61.06	47.94	52.76	57.1	50.54	56.35	56.76	52.01	50.04
Al ₂ O ₃	20.11	19.82	12.66	15.41	19.69	17.64	17.52	17.07	18.38	19.09
Fe ₂ O ₃ (T)	5.25	4.94	12.18	9.19	7.17	6.76	9.49	8.52	10.02	10.04
MnO	0.06	0.06	0.25	0.16	0.049	0.11	0.074	0.091	0.133	0.164
MgO	0.91	0.7	8.63	6.81	1.22	7.24	3.99	3.44	3.88	4.72
CaO	3.59	3.15	14.5	9.11	3.81	13.35	4.23	4.29	7.47	9.92
Na ₂ O	5.36	5.01	2.34	3.51	3.9	3.22	5.91	5.27	4.4	3.76
K ₂ O	4.31	5.08	0.84	1.83	5.69	0.49	0.98	2.41	2.11	1.02
TiO ₂	0.23	0.36	0.78	0.92	0.582	0.443	1.016	0.852	1.213	0.636
P ₂ O ₅	0.21	0.13	0.18	0.35	0.17	0.35	0.43	0.28	0.53	0.32
LOI	0.26	0.2	0.28	0.48	0.21	0.54	-0.04	0.77	0.23	0.07
Total	99.96	100.5	100.6	100.5	99.6	100.7	99.95	99.74	100.4	99.77
Trace and rare earth elements (ppm)										
Sc	2	2	38	29	3	27	19	18	20	21
Be	< 1	< 1	2	2	1	< 1	2	1	1	1
V	165	88	271	206	480	120	186	145	194	149
Cr	< 20	< 20	350	340	< 20	180	30	40	< 20	20
Co	8	6	48	33	16	35	24	22	30	29
Ni	< 20	< 20	70	70	< 20	100	< 20	< 20	< 20	< 20
Cu	20	50	100	10	60	80	50	20	30	40
Zn	80	90	100	90	70	60	40	70	120	100
Ga	22	21	15	18	20	16	22	22	24	20
Ge	1.1	1.2	1.5	2	1.1	1.2	1.4	1.4	1.3	1.3
As	< 5	< 5	< 5	< 5	< 5	< 5	< 5	< 5	< 5	< 5
Rb	35	50	14	47	89	4	18	25	57	18
Sr	1042	796	573	625	1461	1558	364	429	1010	944
Y	5.7	3.6	14.4	21.6	5.3	8.3	23.1	18.4	23.4	13.3
Zr	235	195	73	122	403	37	197	146	198	46
Nb	0.7	2.5	15.6	5.7	6.7	1.5	7.6	6.3	9.2	1.4
Mo	< 2	< 2	< 2	< 2	< 2	< 2	< 2	3	< 2	< 2
Ag	0.9	0.7	< 0.5	0.5	1.5	< 0.5	0.7	0.5	0.7	< 0.5
In	< 0.1	< 0.1	0.1	0.1	< 0.1	< 0.1	< 0.1	< 0.1	0.1	< 0.1
Sn	< 1	1	1	1	1	< 1	1	2	1	1
Sb	< 0.2	< 0.2	< 0.2	< 0.2	< 0.2	< 0.2	< 0.2	< 0.2	< 0.2	< 0.2
Cs	0.7	1.1	0.4	4.6	3.7	< 0.1	0.3	0.2	0.4	0.2

Ba	1920	2007	273	693	6592	391	371	472	1215	620
La	32.2	29.3	21	23.4	17.6	14.3	39.2	37.5	39.7	13.7
Ce	46.5	37.8	57	49.5	28.9	30.4	79.5	71.3	83.9	27.8
Pr	4.22	3.29	8.24	6.16	2.91	3.83	9.16	8.18	10.3	3.55
Nd	14.4	10.7	36.2	26.4	10.1	16.6	36	31.2	42.6	15.9
Sm	2.21	1.37	6.51	5.5	1.59	3.12	6.38	5.51	7.73	3.52
Eu	1.94	1.76	1.69	1.45	0.885	1.07	1.54	1.6	2	1.25
Gd	1.56	0.94	4.58	4.57	1.2	2.41	5.24	4.3	5.92	3.01
Tb	0.19	0.12	0.6	0.7	0.15	0.32	0.75	0.6	0.81	0.46
Dy	0.96	0.62	3.13	4.01	0.84	1.7	4.17	3.35	4.52	2.51
Ho	0.19	0.12	0.57	0.79	0.18	0.29	0.8	0.66	0.84	0.49
Er	0.56	0.37	1.55	2.25	0.61	0.8	2.31	1.93	2.24	1.32
Tm	0.086	0.057	0.212	0.323	0.106	0.11	0.318	0.266	0.312	0.186
Yb	0.62	0.41	1.39	2.04	0.95	0.67	2.06	1.74	1.94	1.13
Lu	0.104	0.067	0.223	0.333	0.189	0.101	0.317	0.277	0.304	0.183
Hf	5	4.2	1.9	3.3	10.3	1.2	4.8	3.7	4.5	1.2
Ta	0.04	0.14	0.58	0.26	0.38	0.04	0.37	0.3	0.28	0.04
W	0.6	0.6	0.5	0.9	0.6	< 0.5	0.8	2.4	< 0.5	0.9
Tl	0.22	0.3	0.11	0.23	0.46	< 0.05	0.08	0.13	0.27	0.15
Pb	19	20	< 5	7	16	< 5	< 5	< 5	8	6
Bi	< 0.1	< 0.1	< 0.1	< 0.1	< 0.1	< 0.1	< 0.1	0.1	< 0.1	< 0.1
Th	0.36	0.39	0.88	0.7	0.84	0.17	2.85	1.23	0.51	0.06
U	0.18	0.17	0.2	0.35	0.76	0.07	1.17	0.38	0.36	0.06

Tab. S2: Raman data for quartz inclusions in garnet. Measured peak positions, shift between sample and standard and calculated pressure for Raman bands 464 and 128.

Sample	Measurement #	464 band					128 band				
		Measured position (cm ⁻¹)	Uncertainty	Measured position for the standard (cm ⁻¹)	Shift (cm ⁻¹)	Pressure (Gpa)	Measured position (cm ⁻¹)	Uncertainty	Measured position for the standard (cm ⁻¹)	Shift (cm ⁻¹)	Pressure (GPa)
HAM-1	1	464.86	0.46	463.95	0.91	0.10	126.77	0.29	126.12	0.65	0.09
HAM-1	2	465.33	0.51	463.95	1.38	0.15	127.14	0.53	126.12	1.02	0.14
HAM-1	3	465.23	0.24	463.95	1.28	0.14	126.29	0.24	126.12	0.17	0.02
HAM-1	4	465.23	0.14	463.95	1.28	0.14	126.60	0.21	126.12	0.47	0.06
HAM-1	5	464.97	0.37	463.95	1.02	0.11	126.79	0.52	126.12	0.67	0.09
HAM-1	6	465.39	0.38	463.74	1.65	0.18	126.83	0.34	126.09	0.74	0.10
HAM-1	7	464.80	0.26	463.74	1.06	0.12	126.60	0.16	126.09	0.51	0.07
HAM-1	8	465.15	0.16	463.74	1.41	0.16	126.91	0.24	126.09	0.82	0.11
HAM-1	9	465.11	0.16	463.74	1.36	0.15	126.75	0.29	126.09	0.66	0.09
HAM-1	10	465.79	0.13	463.94	1.86	0.21	127.49	0.30	126.80	0.69	0.09
HAM-1	11	465.43	0.19	463.94	1.49	0.17	127.54	0.22	126.80	0.74	0.10
HAM-1	12	465.17	0.33	463.94	1.23	0.14	127.27	0.36	126.80	0.47	0.06
HAM-2	1	467.12	0.18	464.35	2.76	0.31	128.93	0.21	127.24	1.68	0.23
HAM-2	2	465.74	0.14	464.35	1.39	0.15	127.98	0.24	127.24	0.73	0.10
HAM-2	4	464.74	0.33	463.47	1.27	0.14	126.81	0.30	126.03	0.78	0.11
HAM-2	5	466.17	0.30	463.47	2.70	0.30	128.03	0.47	126.03	2.00	0.28
HAM-2	6	465.60	0.46	463.47	2.14	0.24	127.77	0.98	126.03	1.74	0.24
HAM-2	7	466.35	0.20	463.47	2.88	0.32	128.24	0.23	126.03	2.21	0.31
HAM-2	8	465.42	0.20	463.47	1.95	0.22	127.41	0.27	126.03	1.38	0.19
HAM-2	9	465.29	0.21	463.47	1.82	0.20	127.00	0.19	126.03	0.97	0.13
HAM-2	10	467.00	0.21	464.35	2.64	0.30	128.44	0.30	127.24	1.20	0.16
HAM-2	11	466.10	0.37	464.60	1.51	0.17	127.99	0.21	127.46	0.53	0.07

5. Additional references:

- Angel, R. J., Alvaro, M., Miletich, R., and Nestola, F., 2017, A simple and generalised P–T–V EoS for continuous phase transitions, implemented in EosFit and applied to quartz: *Contributions to Mineralogy and Petrology*, v. 172, no. 5, p. 29.
- Bachmann, F., Hielscher, R., and Schaeben, H., 2010, Texture analysis with MTEX–free and open source software toolbox: *Solid State Phenomena*, v. 160, p. 63–68.
- Gonzalez, J.P., Thomas, J.B., Baldwin, S.L., and Alvaro, M. (2019) Quartz-in-garnet and Ti-in-quartz thermobarometry: Methodology and first application to a quartzofeldspathic gneiss from eastern Papua New Guinea. *Journal of Metamorphic Geology*, 37, 1193–1208.
- Middlemost, E. A., 1994, Naming materials in the magma/igneous rock system: *Earth-Science Reviews*, v. 37, no. 3-4, p. 215-224.
- Murri, M., Mazzucchelli, M.L., Campomenosi, N., Korsakov, A. V., Prencipe, M., Mihailova, B.D., Scambelluri, M., Angel, R.J., and Alvaro, M. (2018) Raman elastic geobarometry for anisotropic mineral inclusions. *American Mineralogist*, 113, 1869–1872.
- Milani, S., Nestola, F., Alvaro, M., Pasqual, D., Mazzucchelli, M., Domeneghetti, M., and Geiger, C., 2015, Diamond–garnet geobarometry: The role of garnet compressibility and expansivity: *Lithos*, v. 227, p. 140-147.